TRENDS IN SCIENCES 2026; 23(10): 13418
https://doi.org/10.48048/tis.2026.13418 RESEARCH ARTICLE

High-Capacity Removal of Lead and Cadmium Using FGD Gypsum-Derived Hydroxyapatite: Kinetic and Equilibrium Adsorption Studies

Sukrit Sarati[1,2], Uraiwan Intatha[1,2], Sitthi Duangphet[1,2], Nattakan Soykeabkaew[1,2] and Nattaya Tawichai[1,2,*]

[1]School of Science, Mae Fah Luang University, Chiang Rai 57100, Thailand
[2]Center of Innovative Materials for Sustainability, Mae Fah Luang University, Chiang Rai 57100, Thailand

([*]Corresponding author's e-mail: nattaya.taw@mfu.ac.th)

Received: 21 January 2026, Revised: 9 March 2026, Accepted: 20 March 2026, Published: 30 April 2026

Abstract

Power plant FGD gypsum was successfully valorized into high-purity hydroxyapatite (FGD-HAP) via a hydrothermal route at 150 °C. Structural and textural analyses confirmed the formation of well-crystallized hexagonal hydroxyapatite with a phase purity of 93.9% and a mesoporous morphology favorable for adsorption processes. Batch adsorption experiments demonstrated exceptional removal efficiencies toward Pb^{2+} and Cd^{2+} ions, achieving maximum adsorption capacities of 312.5 and 57.47 mg/g, respectively. Kinetic data were best described by the pseudo-second-order model, while equilibrium data fitted well with the Langmuir isotherm, indicating monolayer adsorption. Mechanistic analysis based on the Dubinin-Radushkevich model revealed that Pb^{2+} removal was dominated by ion exchange and surface chemical interactions, whereas Cd^{2+} adsorption was governed primarily by physical adsorption. These findings highlight FGD gypsum as a sustainable and highly effective precursor for advanced adsorbents, offering a promising circular-economy solution for heavy-metal remediation in water treatment applications.

Keywords: Hydroxyapatite, Flue gas desulfurization gypsum, FGD, Adsorption, Heavy metals, Hydrothermal

Introduction

Heavy metals, particularly cadmium (Cd^{2+}) and lead (Pb^{2+}), are among the most hazardous contaminants in industrial wastewater due to their toxicity, non-biodegradability, and ability to accumulate in living organisms [1]. Excessive intake of Cd^{2+} may cause renal dysfunction, skeletal disorders, and cancer, while Pb^{2+} exposure adversely affects the nervous and cardiovascular systems [2]. According to the U.S. EPA and the World Health Organization, the permissible limits of Cd^{2+} and Pb^{2+} in water are extremely low, reflecting the urgent need for effective removal before discharge into the environment [3]. Various physical and chemical technologies, such as coagulation, ion exchange, membrane separation, and photocatalysis, have been used for removing heavy metals, yet many remain costly or inefficient at low metal concentrations [4,5]. Adsorption has emerged as a more practical and economical option due to its high efficiency, simplicity, and minimal sludge production [6].

Hydroxyapatite (HAP, $Ca_{10}(PO_4)_6(OH)_2$) has gained significant attention as an adsorbent because of its high affinity for metal ions, low solubility, and stability under a wide range of environmental conditions. Numerous studies have reported excellent adsorption of Pb^{2+}, Cd^{2+}, Cu^{2+}, Ni^{2+}, and other metal ions using synthetic HAP and HAP-based composites [7-9]. However, conventional HAP synthesis often relies on expensive calcium precursors, such as calcium nitrate or calcium chloride, thereby increasing overall production costs [10]. This has encouraged researchers to explore low-cost alternative calcium sources, particularly industrial by-products.

Flue gas desulfurization (FGD) gypsum, a by-product obtained from coal-fired power plants during SO_2 removal, is primarily composed of $CaSO_4 \cdot 2H_2O$

and is generated in massive quantities in Thailand, for example, the Mae Moh power plant produces an oversupply of FGD gypsum annually, much of which is disposed of in landfills, causing land occupation, dust emissions, and secondary environmental issues. Converting FGD gypsum into valuable products offers both environmental and economic opportunities within the circular economy framework. Recent studies have demonstrated that FGD gypsum can serve as an ideal calcium source for synthesizing hydroxyapatite through wet chemical or hydrothermal routes, and FGD-derived HAP has shown promising adsorption performance for Pb^{2+}, Cd^{2+}, and Cu^{2+} [1,6,11]. Nevertheless, further studies are needed to optimize synthesis conditions and evaluate adsorption mechanisms in depth.

Despite the growing number of studies reporting the conversion of FGD gypsum into hydroxyapatite, several critical aspects remain insufficiently explored. In particular, systematic correlations among phase purity, surface characteristics, and metal-specific adsorption mechanisms remain limited. Moreover, comparative investigations that clearly distinguish the adsorption behaviors of Pb^{2+} and Cd^{2+} on FGD-derived hydroxyapatite under identical experimental conditions remain scarce. Addressing these gaps is essential for advancing the practical application of FGD-HAP in real wastewater treatment systems.

Therefore, this research focuses on synthesizing hydroxyapatite from FGD gypsum via a hydrothermal process and evaluating its performance in adsorbing Cd^{2+} and Pb^{2+}. The synthesized FGD-HAP was characterized using XRD, FTIR, FESEM, and BET analyses to confirm its structural and textural properties. The adsorption behavior was assessed through batch experiments, and Cd^{2+} and Pb^{2+} concentrations were quantified using ICP-MS/MS. This work aims to establish FGD gypsum as a sustainable precursor for the production of high-performance adsorbents, supporting both industrial waste valorization and environmental remediation.

Materials and methods

Materials

The FGD gypsum was supplied by the Mae Mao power plant in Lampang Province, Thailand. Absolute Ethanol 99%, $Pb(NO_3)_2$, $Cd(NO_3)_2.4H_2O$, $(NH_4)2HPO_4$, $NH_3 \cdot H_2O$, purchased from Thailand Chemical Reagent Company, are all analytical grade. Simulated stock wastewaters with 1,000 mg/L were prepared by respectively dissolving appropriate amounts of $Pb(NO_3)_2$ and $Cd(NO_3)_2$ in deionized (DI) Water. The desired concentrations in experiments were prepared by diluting stock wastewaters.

Preparation of FGD powder

The FGD gypsum from the Mae Moh power plant in Lampang Province, Thailand, was subjected to ball milling in deionized (DI) water for 24 h. After milling, the material was dried in an oven at 60 °C for 2 h. The dried gypsum was then sieved using a 45 μm mesh to obtain FGD powder of particle size ≤ 45 μm, which was subsequently used in the synthesis of FGD-HAP. The elemental composition of the sieved FGD powder was analyzed by Micro X-ray fluorescence (Micro XRF) (Bruker/M4 Tornado, Germany).

FGD-HAP synthesis by the Hydrothermal method

The synthesis of FGD-HAP was carried out via a hydrothermal method. Initially, FGD gypsum and $(NH_4)_2HPO_4$ were mixed in 50 mL of deionized (DI) water at room temperature, maintaining a calcium-to-phosphorus (C/P) molar ratio of 1.67. The pH of the resulting suspension was adjusted to 10 - 11 by the gradual addition of $NH_3 \cdot H_2O$, and the mixture was vigorously stirred for 30 min to ensure homogeneity. After stirring, the mixture was transferred into a Teflon-lined stainless-steel autoclave and subjected to hydrothermal treatment in an oven at 150 °C for 24 h. Upon completion, the autoclave was allowed to cool to room temperature. The solid product obtained was then washed sequentially with 50 mL of DI water twice and 50 mL of ethanol once to remove impurities, and then dried at 80 °C for 12 h. The dried sample was subsequently ground and sieved through a 45 μm mesh to obtain a fine FGD-HAP powder.

Characterization

The chemical composition of FGD gypsum was determined through quantitative analysis of X-ray fluorescence (XRF). A representative sample was analyzed using a Bruker/M4 Tornado in Germany to identify major and minor elements. The crystalline phases of the synthesized FGD-HAP were analyzed

using X-ray diffraction (XRD) with a PANalytical/Empyrean diffractometer (Netherlands) equipped with a Cu-Kα radiation source. The samples were prepared as fine powders and scanned over a typical 2θ range of 10° - 60° to identify the crystalline phases present. The obtained diffraction patterns were compared with standard reference databases to confirm the formation of hydroxyapatite and to detect any secondary phases originating from FGD gypsum. In addition, the Rietveld refinement method in HighScore was employed to assess phase purity.

Fourier Transform Infrared Spectroscopy (Raman Spectrometer) (FTIR) was conducted to investigate the functional groups and bonding characteristics of both the raw FGD gypsum and the synthesized FGD-HAP. The analysis was performed using a Thermo Scientific/Nicolet iS50 instrument over the spectral range of 4,000 - 400 cm^{-1}.

The surface area and pore characteristics of the synthesized FGD-HAP were analyzed using the Brunauer-Emmett-Teller (BET) method with a Quantachrome® ASiQwin™ instrument. Prior to analysis, the samples were degassed at 120 °C for 12 h to remove moisture and adsorbed impurities.

Field Emission Scanning Electron Microscope (FESEM) analysis was performed to investigate the surface morphology, composition, and microstructure of the synthesized FGD-HAP. A TESCAN/MIRA instrument was used, and images were captured at a magnification of 150,000x.

Batch adsorption experiments

The adsorption experiments for Pb^{2+} and Cd^{2+} were carried out using the batch method. The conical flasks containing 0.05 g FGD-HAP and 50 mL of the heavy metal solution at the desired concentration were placed in an Incubator Shaker (Shellab/SI4-2) at 200 rpm and a constant room temperature (25°C). The initial concentrations of the Pb^{2+} solutions were prepared at 30, 40, 50, 100, 200, 300, 400, and 500 mg/L, whereas the Cd^{2+} solutions were prepared at 30, 40, and 50 mg/L at pH 5.5 ± 0.1 to prevent metal precipitation while ensuring optimal adsorption. Contact times of 1, 2 and 3 h were employed to investigate the influence of adsorption time on the removal efficiency of both metal ions. After adsorption, the mixtures were filtered through a membrane filter (Whatman Grade 4, 20 - 25 μm), and the filtrates were analyzed for residual metal (Pb^{2+} and Cd^{2+}) concentration by Inductively Coupled Plasma Triple-quadrupole Mass Spectrometer (ICP-MS/MS) (Agilent Technologies/8900 Triple Quadrupole ICP-MS). All adsorption experiments were performed in triplicate. The amounts of lead and cadmium adsorbed, and the removal percentages of lead and cadmium were calculated using Eqs. (1) and (2), respectively.

$$q_t \frac{(C_0 - C_t)V}{m} \quad (1)$$

$$\%\, Removal = \frac{(C_0 - C_t)}{C_0 \times 100} \quad (2)$$

where q_t (mg/g) are the adsorption capacities at time t, C_0 and C_t (mg/L) are the single-metal concentrations in the initial solution and at time t, respectively; V (L) is the volume of solution, and m (g) is the weight of the sample added to the solution. Adsorption kinetics of Pb^{2+} and Cd^{2+} were both studied in the range of 1 - 3 h. Adsorption isotherms were investigated over the ranges of 30 - 500 mg/L for Pb^{2+} and 30 - 50 mg/L for Cd^{2+}.

Results and discussion

The physical and chemical characterization of the precursor material (FGD gypsum) and the final product (FGD-HAP) was conducted to validate the synthesis process and identify the key properties of the adsorbent. The quantitative chemical composition of the major elements present in FGD gypsum was determined by X-ray fluorescence (XRF) analysis, as shown in **Table 1**.

Table 1 Chemical composition of FGD gypsum by XRF.

Composition	Value (wt.%)
Calcium	54.07
Sulfur	43.85
Silicon	0.59
Magnesium	0.50
Aluminium	0.44
Iron	0.38
Chromium	0.07
Strontium	0.06
Manganese	0.04

The XRF analysis revealed that the FGD gypsum consisted predominantly of calcium (54.07 wt%) and sulfur (43.85 wt%), which is consistent with the typical composition of synthetic gypsum produced from flue gas desulfurization processes. The high calcium and sulfur contents indicate that the material is primarily composed of calcium sulfate ($CaSO_4 \cdot 2H_2O$), confirming its suitability as a precursor for the synthesis of calcium-rich materials, such as hydroxyapatite (HAP). Minor elements, including Si, Mg, Al, Fe, Cr, Sr, and Mn, were present in small quantities (< 1 wt%), suggesting that the FGD gypsum contains trace impurities commonly derived from coal combustion residues or additives used in desulfurization units. These impurities are unlikely to significantly affect the HAP synthesis but may influence certain material properties such as crystallinity, nucleation behavior, or colour. The exceptionally high calcium content, relative to other elements, supports its use in HAP synthesis with a controlled Ca/P ratio of 1.67, ensuring that sufficient Ca^{2+} ions are available for the formation of stoichiometric hydroxyapatite. Overall, the chemical profile confirms that this FGD gypsum is a chemically suitable and resource-efficient waste material for conversion into value-added calcium phosphate products.

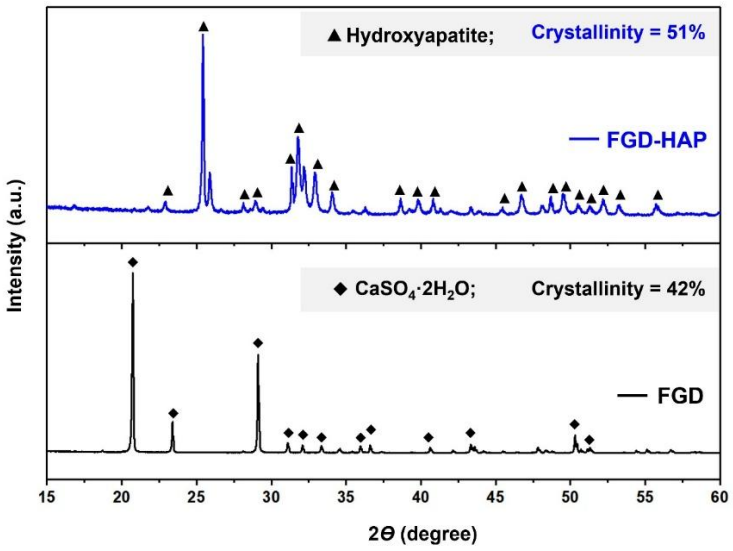

Figure 1 Diffraction profiles comparing FGD gypsum precursor in dihydrate ($CaSO_4 \cdot 2H_2O$) with the synthesized FGD-HAP matched hydroxyapatite reference confirm the successful conversion from FGD gypsum to hydroxyapatite.

The wide-angle XRD pattern of FGD-HAP in **Figure 1** shows the crystalline phases present in the materials and confirms whether the precursor successfully transformed into the desired FGD-HAP structure during synthesis. Fourteen characteristic hydroxyapatite peaks were observed at 2θ = 10.833°,

25.868°, 28.924°, 31.765°, 32.184°, 32.900°, 34.053°, 39.795°, 46.689°, 48.076°, 49.472°, 50.478°, 52.071°, and 53.186°. These diffraction peaks match well with PDF No. 96-900-2217, confirming that the FGD-HAP possesses a hexagonal $P6_3/m$ crystal structure with lattice constants a = b = 9.423 Å and c = 6.883 Å. The crystallite size, calculated using the Scherrer equation, was 61 nm. Furthermore, the phase purity of the synthesized hydroxyapatite was determined by Rietveld refinement in HighScore software. The high phase purity (93.9%) obtained from Rietveld refinement indicates that the hydrothermal conversion of FGD gypsum effectively suppressed the formation of secondary calcium phosphate phases. This high crystallinity is expected to enhance ion-exchange efficiency by providing well-defined Ca^{2+} lattice sites, which is particularly advantageous for Pb^{2+} removal.

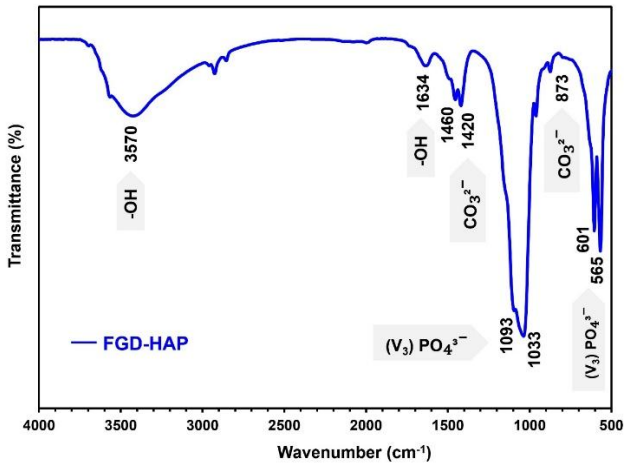

Figure 2 FTIR spectrum of the synthesized FGD-HAP. Characteristic absorption bands confirm the successful hydrothermal conversion of FGD gypsum into hydroxyapatite.

FTIR spectra of FGD-HAP are presented in **Figure 2**. The absorption bands at 1,093, 1,033, 962, 601, and 565 cm^{-1} correspond to the vibrational modes of phosphate (PO_4^{3-}) groups [12,13]. The peaks at 3,570 and 634 cm^{-1} are indicative of hydroxyl (OH^-) groups [14], supporting the role of surface hydroxyls in metal-ion adsorption through surface complexation. A bimodal band at 1,460 and 1,420 cm^{-1}, together with a single peak at 873 cm^{-1}, is assigned to carbonate (CO_3^{2-}) groups, indicating partial substitution of phosphate by carbonate during air exposure of FGD-HAP [15,16]. In addition, 2 weak, broad bands at 3,450 and 1,637 cm^{-1} are attributed to adsorbed water molecules on the sample surface. These spectral features indicated the chemical change from FGD gypsum to fully developed hydroxyapatite.

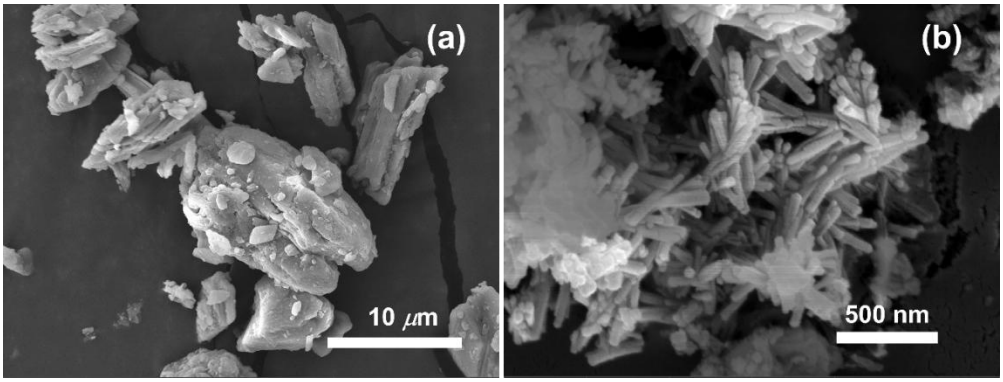

Figure 3 SEM micrographs illustrating the morphological evolution from (a) raw FGD gypsum to (b) synthesized FGD-HAP.

To observe particle morphology, surface texture, and structural changes, providing visual evidence of how the material evolved from the precursor to the final FGD-HAP product. **Figure 3** shows the SEM images of raw FGD and FGD-HAP powders. The raw FGD particles appear as relatively large platy and tabular morphology, which is the typical crystal habit of gypsum. The FGD-HAP particles, with diameters ranging from 15 - 25 nm and lengths of 100 - 250 nm, exhibit a uniform rod-like morphology. Most particles tend to aggregate, likely due to the fusion or partial melting of their surfaces, which promotes particle - particle attachment. The transition from the massive, blocky gypsum into the fine, elongated nanostructures indicates that the calcium source was effectively utilized to build the HAP lattice. The interlaced nanorods create a highly porous network, as they vastly increase the available surface area.

Table 2 BET properties of FGD-HAP.

Sample	BET surface area (m^2/g)	Total pore volume (cm^3/g)	Micropore volume (cm^3/g)
FGD-HAP [This study]	35.359	0.092	0.0205
HAP [17,18]	20 - 120	0.10 - 0.30	0.015 - 0.030
FGD [19]	9.41	0.02	-

The textural properties of FGD-HAP are presented in **Table 2**. As shown, the FGD-HAP exhibits a mesoporous structure, with a specific surface area within the typical range reported for hydroxyapatite and a large pore volume. These features are highly beneficial for enhancing ion-exchange capacity and diffusion, ultimately improving the material's adsorption performance [20].

Sorption kinetics

Sorption kinetics were investigated to determine the rate of metal uptake and identify the mechanism controlling adsorption. The experimental data were fitted to kinetic models to determine the rates of interaction between Pb^{2+} and Cd^{2+} and the adsorbent surface.

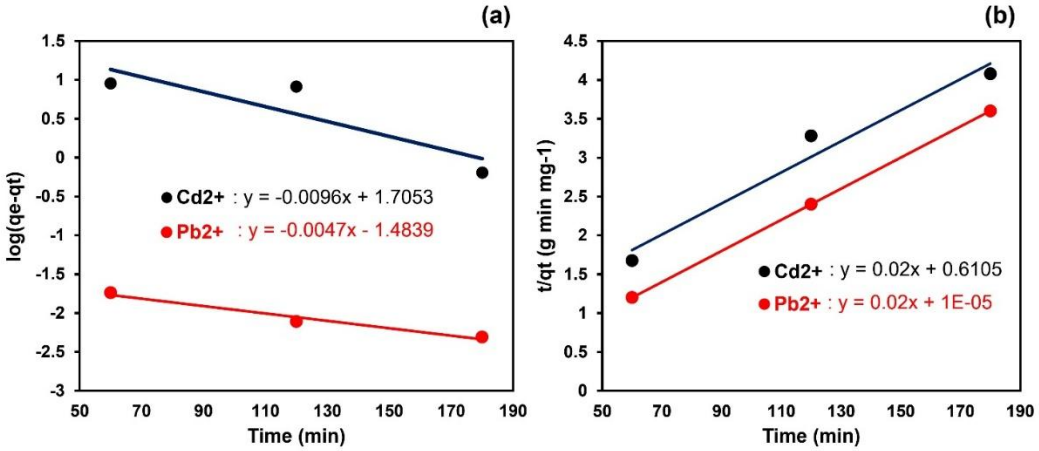

Figure 4 Adsorption kinetics of Pb^{2+} and Cd^{2+} onto synthesized FGD-HAP: (a) pseudo-first order kinetic plots, (b) pseudo-second order kinetic plots.

Sorption kinetics reveal rapid initial uptake of both Pb^{2+} and Cd^{2+} within the first 60 min, driven by abundant active sites on the FGD-HAP surface, followed by gradual saturation and equilibrium at 180 min (**Figure 4**). Experimental capacities reached ~195.5 mg/g for Pb^{2+} and ~44.2 mg/g for Cd^{2+}. To gain deeper insights into the controlling mechanisms of the adsorption process, including mass transfer and chemical reaction effects, the pseudo-first-order and pseudo-second-order kinetic models [21,22] were applied to analyze the experimental data. The linearized forms of these models are expressed as follows:

Pseudo-first-order model

$$\log(q_e - q_t) = log q_e - \frac{k_1 t}{2.303} \quad (3)$$

Pseudo-second-order model

$$\frac{t}{q_t} = \frac{1}{k_2 q_2^2} + \frac{t}{q_e} \quad (4)$$

where q_e and q_t represent the adsorption capacities (mg/g) at equilibrium and at time t (min), respectively; k_1 (min^{-1}) and k_2 (g/(mg·min)) are the rate constants for the pseudo-first-order and pseudo-second-order models. Additionally, when $t \rightarrow 0$, $t \rightarrow 0$, the initial adsorption rate h (mg/(g·min)) can be defined as:

$$h = k_2 q_e^2 \quad (5)$$

Figure 4(a) presents linearized pseudo-first-order plots of $\log(q_e - q_t)$ versus t, which assumes adsorption control by physisorption or film diffusion. These show moderate linearity for Pb^{2+} ($R^2 = 0.996$) but poor fit for Cd^{2+} ($R^2 = 0.777$), with calculated q_e values (203.56 mg/g for Pb^{2+} and 50.73 mg/g for Cd^{2+}) deviating from experimental data. In contrast, **Figure 4(b)** shows pseudo-second-order plots of t/q_t versus t, suggesting chemisorption via valence electron sharing as the rate-limiting step. Both metals yield excellent linearity (Pb^{2+} $R^2 = 1.000$; Cd^{2+} $R^2 = 0.964$), with calculated q_e (200 mg/g for Pb^{2+} and 50.00 mg/g for Cd^{2+}) closely matching measurements. The higher rate constant K_2 for Pb^{2+} (19.23×10^{-3} g/mg·min) versus Cd^{2+} (6.55×10^{-4} g/mg·min) reflecting stronger chemical affinity and faster surface reaction. These findings indicate that the adsorption behaviours of Pb^{2+} and Cd^{2+} are best described by the pseudo-second-order kinetic model, suggesting that the rate-limiting step in the adsorption process is chemical adsorption.

Table 3 Pseudo-first order and pseudo-second order kinetic parameters for the adsorption of Pb^{2+} and Cd^{2+} on FGD-HAP.

Metals	$q_{e,exp}$ (mg/g)	pseudo-first order kinetic model			pseudo-second order kinetic model		
		K_1 (min^{-1})	$q_{e,cal}$ (mg/g)	R^2	K_2 (g/mg min)	$q_{e,cal}$ (mg/g)	R^2
Pb^{2+}	195.5	5.07×10^{-3}	203.56	0.9961	19.23×10^{-3}	200	1
Cd^{2+}	44.156	0.0221	50.73	0.7765	6.55×10^{-4}	50.00	0.9638

Sorption isotherm

Sorption isotherms were analyzed to characterize the adsorbent's equilibrium behavior and adsorption capacity at various initial metal concentrations. The isotherm models provide insight into the interactions between Pb^{2+}/Cd^{2+} ions and the adsorbent surface.

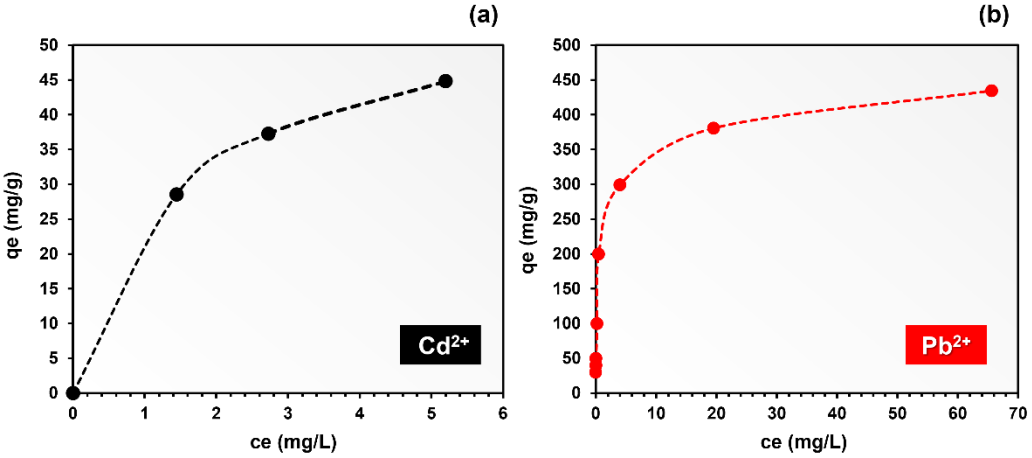

Figure 5 Adsorption isotherms of (a) Cd^{2+} and (b) Pb^{2+} onto FGD-HAP at room temperature showing the relationship between the equilibrium adsorption capacity (q_e) and the equilibrium concentration (C_e).

Adsorption equilibrium data, expressed as the mass of adsorbate adsorbed per unit weight of adsorbent (q_e) versus the equilibrium concentration of the adsorbate in solution (C_e), are commonly represented by adsorption isotherms. These isotherms are essential for practical adsorbent design and for predicting the maximum adsorption capacity. In this study, the adsorption isotherms of Pb^{2+} and Cd^{2+} on FGD-HAP are presented in **Figure 5**. It can be observed that the adsorption capacities of both metals initially increased with equilibrium concentration and subsequently reached saturation. The uptake of Pb^{2+} was consistently higher than that of Cd^{2+}, indicating a stronger interaction between FGD-HAP and Pb^{2+} compared to Cd^{2+}. To better understand the adsorption behaviours, the Langmuir and the Freundlich models were applied to fit the experimental equilibrium data.

Langmuir isotherm

The Langmuir model [23] assumes adsorption occurs on a homogeneous surface with no interaction between adsorbed species. The Langmuir equation is expressed as:

$$\frac{C_e}{q_e} = \frac{C_e}{q_{max}} + \frac{1}{bq_{max}} \quad (6)$$

where C_e is the equilibrium concentration of Pb^{2+} or Cd^{2+} (mg/L), q_e is the amount adsorbed at equilibrium (mg/g), q_{max} is the maximum adsorption capacity (mg/g), and b is the Langmuir constant related to the affinity of binding sites and adsorption energy (L/g).

Freundlich isotherm

The Freundlich model [24] is commonly used to describe adsorption on heterogeneous surfaces. The Freundlich equation is expressed as:

$$logq_e = logK_F + \frac{1}{n} logC_e \quad (7)$$

where K_F is the Freundlich constant representing the adsorption capacity (mg/g(1/mg1/n)), and n is the Freundlich exponent indicating the favourability of the adsorption process. In this study, the n values for Pb^{2+} and Cd^{2+} were 2.85 and 2.845, respectively, indicating favourable adsorption and high affinity between FGD-HAP and the metal ions. The R^2 values show that the Langmuir model better describes the adsorption of both Pb^{2+} and Cd^{2+} (Table 4). With $R^2 \geq 0.985$, the Langmuir isotherm fits best, suggesting monolayer coverage on uniform sites, with maximum adsorption capacities (qmax) of 312.5 mg/g for Pb^{2+} and 53.19 mg/g for Cd^{2+}.

Dubinin-Radushkevich (D-R) isotherm

To further evaluate the adsorption mechanism and to distinguish between physisorption and chemisorption, the Dubinin-Radushkevich (D-R) model [25] was applied. The linear form of the D-R model is expressed as:

$$\ln q_e = \ln q_m - \beta\varepsilon^2 \quad (8)$$

where q_m is the theoretical saturation adsorption capacity (mg/g), β is a constant related to the mean free energy of adsorption (mol^2/J^2), and ε is the Polanyi potential, calculated as:

$$\varepsilon = RT \ln(1 + \frac{1}{C_e}) \quad (9)$$

where R is the universal gas constant (8.3145 J/mol·K), and T is the absolute temperature (K). The mean free energy E of adsorption per mole of sorbate can be calculated by:

$$E = \frac{1}{\sqrt{2\beta}} \quad (10)$$

The E value can predict the type of adsorption: if $E < 8$ kJ/mol, the adsorption is physical; 8 - 16 kJ/mol indicates ion exchange; and $E > 16$ kJ/mol suggests chemisorption stronger than ion exchange [26]. In this study, the E values of Pb^{2+} and Cd^{2+} were 10 and 1.29 kJ/mol, respectively, indicating that the main adsorption mechanism of Pb^{2+} is ion exchange, whereas that of Cd^{2+} is predominantly physical adsorption. The metal ions were likely adsorbed via the exchange of Ca^{2+} in FGD-HAP with Pb^{2+}, while Cd^{2+} was adsorbed mainly on the surface of the adsorbent from the wastewater. In addition, some chemical reactions may occur on the surface of FGD-HAP for Pb^{2+} removal.

Table 4 Langmuir, Freundlich, and Dubinin-Radushkevich parameters for the adsorption of Pb^{2+} and Cd^{2+} onto FGD-HAP.

Metals	Langmuir model			Freundlich model			D-R model		
	q_{max} (mg/g)	b (L/mg)	R^2	K_F (mg/g(1/mg$^{1/n}$))	n	R^2	q_m (mg/g)	E (kJ/mol)	R^2
Pb^{2+}	312.5	5.33	0.9856	203.8	2.85	0.9667	243	10	0.7742
Cd^{2+}	57.47	0.682	1	25.46	2.845	0.9877	45.98	1.29	0.9772

Removal efficiency

This section is intended to evaluate the adsorption performance of the synthesized adsorbent by analysing its removal efficiency for both lead and cadmium under varying initial concentrations. The assessment of removal efficiency is crucial as it provides valuable insights into the material's capacity and effectiveness in lowering metal ion concentrations, as well as the impact of pollutant loading on the overall adsorption dynamics. The removal efficiencies of Cd^{2+} and Pb^{2+} on FGD-HAP at different initial concentrations and contact times are shown in **Figure 6**. The adsorption of Cd^{2+} is strongly dependent on both contact time and initial concentration. As shown in **Figure 6(a)**, the removal percentage of Cd^{2+} increased with contact time across all concentrations tested. At 60 min, the removal efficiencies were 82.5%, 75.6%, and 71.6% for initial concentrations of 30, 40, and 50 mg/L, respectively. After 120 min, the efficiencies increased to 84.5%, 78.3%, and 73.2%, and further reached 91.7%, 91.7%, and 88.3% at 180 min. These results indicate that longer contact times enhance Cd^{2+} adsorption by allowing more time for ions to diffuse and interact with active sites on the FGD-HAP surface. Furthermore, lower initial concentrations yielded higher removal percentages, likely due to greater availability of adsorption sites per ion. In contrast, Pb^{2+} exhibited nearly complete removal under all tested conditions, as shown in **Figure 6(b)**.

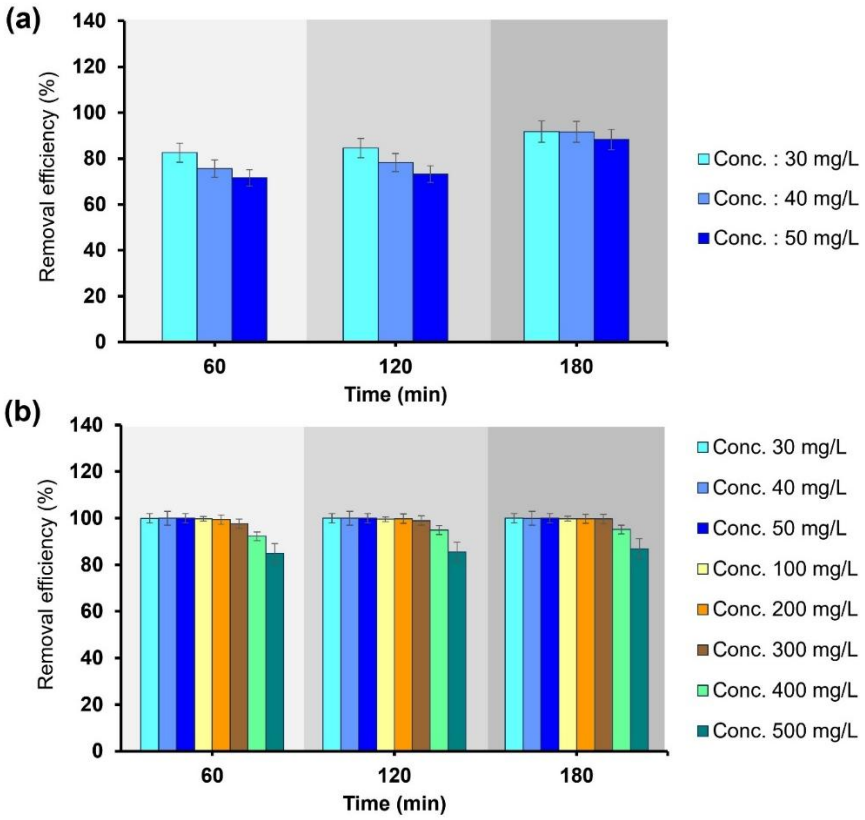

Figure 6 Removal efficiency of (a) Cd^{2+}, and (b) Pb^{2+} onto FGD-HAP as a function of initial concentration and contact time.

The removal efficiency of Pb by the adsorbent was evaluated at initial concentrations of 30, 40, 50, 100, 200, 300, 400, and 500 mg/L, with contact times of 60, 120, and 180 min. The results show that the adsorbent exhibited very high Pb removal efficiency, especially at low to moderate initial concentrations. For initial concentrations of 30 - 100 mg/L, the removal efficiency remained remarkably high, ranging from 99% to 100% across all contact times. This indicates that the adsorbent achieved near-complete Pb removal within the first 60 min, with no significant change throughout the adsorption period. At higher initial concentrations of 200 and 300 mg/L, the Pb removal efficiency remained high (97% - 99%) and increased slightly with longer contact time from 60 to 180 min, suggesting that sufficient adsorption sites were still available. However, when the initial concentration increased to 400 mg/L, the removal efficiency decreased slightly to approximately 92% - 95%, implying that the adsorbent was approaching saturation under higher pollutant loading. At the highest concentration of 500 mg/L, the removal efficiency showed the most notable reduction, with values between 85% and 87%. Although still considered effective, the adsorption performance was clearly affected by the limited availability of adsorption sites at elevated Pb concentrations.

Table 5 presents a comparison of the maximum adsorption capacities (q_{max}) of Pb^{2+} and Cd^{2+} across various adsorbents. FGD-HAP exhibits an exceptionally high adsorption capacity for Pb^{2+}, whereas its q_{max} for Cd^{2+} is comparable to those of other adsorbents. These results indicate that FGD-HAP is a highly effective adsorbent for removing both metal ions, with particularly outstanding performance for Pb^{2+}. Therefore, hydroxyapatite synthesized from FGD waste is a promising and efficient material for removing Pb^{2+} and Cd^{2+} from aqueous solutions.

Table 5 Comparison of maximum adsorption capacity (q_{max}) for Pb^{2+} and Cd^{2+} with various adsorbents.

Metals	Adsorbents	q_{max} (mg/g)
Pb^{2+}	FGD-HAP [This study]	312.5
	FGD-HAP [6]	277.8
	H_2O_2 modified biochar [27]	60.87
	Modified orange peel [28]	15.27
	HAP-biochar [29]	134.4
Cd^{2+}	FGD-HAP [This study]	57.47
	FGD-HAP [6]	43.10
	Chicken bone-HAP [30]	22.94
	Corn stalk [31]	0.16
	Fish bone-HAP [32]	54.35

Conclusions

Power plant FGD gypsum was successfully valorized into high-purity (93.9%), well-crystallized hexagonal hydroxyapatite (FGD-HAP) via a hydrothermal route at 150 °C. The synthesized material exhibited a mesoporous morphology and exceptional removal efficiencies, with maximum adsorption capacities of 312.5 mg/g for Pb^{2+} and 57.47 mg/g for Cd^{2+}. The kinetic data for both ions were described by the pseudo-second-order model ($R^2 > 0.96$), signifying rate control by chemical interactions. Equilibrium data conformed to the Langmuir isotherm ($R^2 \geq 0.985$), while the Dubinin-Radushkevich model provided mechanistic clarity, whereas Pb^{2+} adsorption (E = 10 kJ/mol) proceeds primarily via ion exchange coupled with surface chemical reactions, and Cd^{2+} uptake (E = 1.29 kJ/mol) is dominated by physisorption. Overall, hydroxyapatite produced from FGD waste has proven to be a very effective and promising adsorbent for removing Pb^{2+} and Cd^{2+} from water. Its high specific surface area, beneficial pore features, and excellent phase purity support the idea that FGD-HAP is a

sustainable and efficient solution for heavy metal cleanup. Future research should explore how well FGD-HAP adsorbs other heavy metal ions not tested here. Testing its effectiveness with a wider variety of contaminants will help identify which metals it can most effectively remove and the best practical uses for this material in real-world cleanup efforts.

Acknowledgements

This research project was supported by Mae Fah Luang University, Thailand (Fundamental Fund: Fiscal year 2023 by Thailand Science Research and Innovation (TSRI), and National Science Research and Innovation Fund (NSRF).

Declaration of generative AI in scientific writing

The authors acknowledge the use of generative AI tools (e.g., Gemini and ChatGPT by OpenAI) in the preparation of this manuscript, specifically for language editing and grammar correction. No content generation or data interpretation was performed by AI. The authors take full responsibility for the content and conclusions of this work.

CRediT author statement

Sukrit Sarati: Conceptualization, Methodology, Software, Formal analysis, Investigation, Resources, Data Curation, Writing - Original Draft, Visualization. **Uraiwan Intatha**: Validation, Writing - Review & Editing, Supervision. **Sitthi Duangphet:** Validation, Writing - Review & Editing, Supervision. **Nattakan Soykeabkaew:** Validation, Writing - Review & Editing, Supervision. **Nattaya Tawichai:** Conceptualization, Validation, Resources, Writing - Review & Editing, Supervision, Project administration, Funding acquisition.

References

[1] Y Liu, Y Yan, B Seshadri, F Qi, Y Xu, N Bolan, F Zheng, X Sun, W Han and L Wang. Immobilization of lead and copper in aqueous solution and soil using hydroxyapatite derived from flue gas desulphurization gypsum. *Journal of Geochemical Exploration* 2018; **184(B)**, 239-246.

[2] GK Kinuthia, V Ngure, D Beti, R Lugalia, A Wangila and L Kamau. Levels of heavy metals in wastewater and soil samples from open drainage channels in Nairobi, Kenya: Community health implication. *Scientific Reports* 2020; **10(1)**, 8434.

[3] World Health Organization. *A global overview of national regulations and standards for drinking-water quality 2018*. World Health Organization, Geneva, Switzerland, 2018.

[4] T Kikuchi and S Tanaka. Biological removal and recovery of toxic heavy metals in water environment. *Critical Reviews in Environmental Science and Technology* 2012; **42(10)**, 1007-1057.

[5] Z Elouear, J Bouzid, N Boujelben, M Feki, F Jamoussi and A Montiel. Heavy metal removal from aqueous solutions by activated phosphate rock. *Journal of Hazardous Materials* 2008; **156(1)**, 412-420.

[6] Y Yan, X Dong, X Sun, X Sun, J Li, J Shen, W Han, X Liu and L Wang. Conversion of waste FGD gypsum into hydroxyapatite for removal of Pb^{2+} and Cd^{2+} from wastewater. *Journal of Colloid and Interface Science* 2014; **429**, 68-76.

[7] A Corami, S Mignardi and V Ferrini. Cadmium removal from single- and multi-metal (Cd+Pb+Zn+Cu) solutions by sorption on hydroxyapatite. *Journal of Colloid and Interface Science* 2008; **317**, 402-408.

[8] E Mavropoulos, AM Rossi, AM Costa, CAC Perez, JC Moreira and M Saldanha. Studies on the mechanisms of lead immobilization by hydroxyapatite. *Environmental Science & Technology* 2002; **36(7)**, 1625-1629.

[9] M Aliabadi, M Irani, J Ismaeili and S Najafzadeh. Design and evaluation of chitosan/hydroxyapatite composite nanofiber membrane for the removal of heavy metal ions from aqueous solution. *Journal of the Taiwan Institute of Chemical Engineers* 2014; **45(2)**, 518-526.

[10] NM Pu'ad, RA Haq, HM Noh, HZ Abdullah, MI Idris and TC Lee. Synthesis method of hydroxyapatite: A review. *Materials Today: Proceedings* 2020; **29**, 233-239.

[11] S Kiziltas Demir and N Tugrul. Zinc and cadmium adsorption from wastewater using hydroxyapatite synthesized from flue gas desulfurization waste. *Water Science and Technology* 2021; **84(5)**, 1280-1292.

[12] H Zhang, M Liu, H Fan and X Zhang. An efficient method to synthesize carbonated nano

hydroxyapatite assisted by poly (ethylene glycol). *Materials Letters* 2012; **75**, 26-28.

[13] J Di Chen, YJ Wang, K Wei, SH Zhang and XT Shi. Self-organization of hydroxyapatite nanorods through oriented attachment. *Biomaterials* 2007; **28(14)**, 2275-2280.

[14] S Kongsri, K Janpradit, K Buapa, S Techawongstien and S Chanthai. Nanocrystalline hydroxyapatite from fish scale waste: Preparation, characterization and application for selenium adsorption in aqueous solution. *Chemical Engineering Journal* 2013; **215**, 522-532.

[15] DP Minh, ND Tran, A Nzihou and P Sharrock. Calcium phosphate-based materials starting from calcium carbonate and orthophosphoric acid for the removal of lead (II) from an aqueous solution. *Chemical Engineering Journal* 2014; **243**, 280-288.

[16] J Hu, J Russell, B Ben-Nissan and R Vago. Production and analysis of hydroxyapatite from Australian corals via hydrothermal process. *Journal of Materials Science Letters* 2001; **20(1)**, 85-87.

[17] A Fadli, SR Yenti, AP Wisrayetti, J Hasibuan, VG Herjan, A Isnani and R Restyanda. Optimisation of the hydroxyapatite surface area prepared using a porogen rubber suspension. *Ceramics-Silikaty* 2023; **67(3)**, 371-378.

[18] SG Mtavangu, W Mahene, RL Machunda, B van der Bruggen and KN Njau. Cockle (*Anadara granosa*) shells-based hydroxyapatite and its potential for defluoridation of drinking water. *Results in Engineering* 2022; **13**, 100379.

[19] H Ma, A Khalaf, R Chen, Z Wang, Y Li and F Xu. Evaluation of flue gas desulfurization gypsum as a low-cost precipitant for phosphorus removal from anaerobic digestion effluent filtrate. *IOP Conference Series: Earth and Environmental Science* 2023; **1135(1)**, 012011.

[20] F Zhang, Z Zhao, R Tan, W Xu, G Jiang and W Song. Efficient and selective immobilization of Pb^{2+} in highly acidic wastewater using strontium hydroxyapatite nanorods. *Chemical Engineering Journal* 2012; **203**, 110-114.

[21] L Ding, C Wu, H Deng and X Zhang. Adsorptive characteristics of phosphate from aqueous solutions by MIEX resin. *Journal of Colloid and Interface Science* 2012; **376(1)**, 224-232.

[22] YS Ho and G McKay. Pseudo-second order model for sorption processes. *Process Biochemistry* 1999; **34(5)**, 451-465.

[23] I Langmuir. The adsorption of gases on plane surface of glass, mica and platimnum. *Journal of the American Chemical Society* 1918; **40(9)**, 1361-1403.

[24] H Freundlich. Über die adsorption in lösungen. *Zeitschrift für Physikalische Chemie* 1907; **57(1)**, 385-470.

[25] MM Dubinin. The potential theory of adsorption of gases and vapors for adsorbents with energetically nonuniform surfaces. *Chemical Reviews* 1960; **60(2)**, 235-241.

[26] H Demiral, I Demiral, F Tumsek and B Karabacakoglu. Adsorption of chromium (VI) from aqueous solution by activated carbon derived from olive bagasse and applicability of different adsorption models. *Chemical Engineering Journal* 2008; **144(2)**, 188-196.

[27] W Ahmed, S Mehmood, A Núñez-Delgado, S Ali, M Qaswar, A Shakoor, M Mahmood and DY Chen. Enhanced adsorption of aqueous Pb(II) by modified biochar produced through pyrolysis of watermelon seeds. *Science of the Total* Environment 2021; **784**, 147136.

[28] MR Lasheen, NS Ammar and HS Ibrahim. Adsorption/desorption of Cd(II), Cu(II) and Pb(II) using chemically modified orange peel: Equilibrium and kinetic studies. *Solid State Sciences* 2012; **14(2)**, 202-210.

[29] L Sun, J Wu, J Wang, M Xu, W Zhou, Y Du, Y Li and H Li. Fabricating hydroxyapatite functionalized biochar composite using steel slag and Hami melon peel for Pb(II) and Cd(II) removal. *Colloids and Surfaces A: Physicochemical and Engineering Aspects 2023*; **666**, 131310.

[30] R Foroutan, SJ Peighambardoust, SS Hosseini, A Akbari and B Ramavandi. Hydroxyapatite biomaterial production from chicken (femur and beak) and fishbone waste through a chemical less method for Cd^{2+} removal from shipbuilding wastewater. *Journal of Hazardous Materials* 2021; **413**, 125428.

[31] C Phaenark, T Jantrasakul, P Paejaroen, S Chunchob and W Sawangproh. Sugarcane bagasse and corn stalk biomass as a potential sorbent for the removal of Pb(II) and Cd(II) from Aqueous Solutions. *Trends in Sciences* 2023; **20(2)**, 6221.

[32] PL Hariani, A Rachmat, M Said and S Salni. Modification of fishbone-based hydroxyapatite with $MnFe_2O_4$ for efficient adsorption of Cd(II) and Ni(II) from aqueous solution. *Indonesian Journal of Chemistry* 2021; **21**, 1471.